



### Available online at www.sciencedirect.com

# **ScienceDirect**

Journal of Magnesium and Alloys 8 (2020) 1296-1303



www.elsevier.com/locate/jma

# Full Length Article

# Deformation nanomechanics and dislocation quantification at the atomic scale in nanocrystalline magnesium

Md. Shahrier Hasan, Rachell Lee, Wenwu Xu\*

Department of Mechanical Engineering, San Diego State University, San Diego, CA 92182, United States

Received 4 February 2020; received in revised form 1 July 2020; accepted 4 August 2020

Available online 5 October 2020

### **Abstract**

Classical molecular dynamics (MD) simulation method is employed to study the uniaxial tensile deformation of nanocrystalline magnesium (Mg) of varying grain size levels. The mean grain size of the sample is varied from 6.4 nm to 45 nm, with each sample containing about 43 million atoms in the modeling system. The deformation nanomechanics reveals two distinct deformation mechanisms. For larger grain-sized samples, dislocation dominated deformation is observed while, in smaller grain-sized samples, grain boundary-based mechanisms such as grain boundary sliding, grain boundary rotation are observed. The transition of normal and inverse Hall–Petch relation occurs at around 10 nm. Dislocation density quantification shows that the dislocation density in the sample drastically reduces with decreasing grain size. Elastic modulus of nanocrystalline Mg with mean grain size above 20 nm remains comparable to that of the coarse-grained polycrystalline bulk, followed by a rapid reduction below that grain size. The present work reveals the nanomechanics of nanocrystalline Mg, facilitating the design and development of Mg-based nanostructured alloys with superior mechanical properties.

© 2020 Published by Elsevier B.V. on behalf of Chongqing University.

This is an open access article under the CC BY-NC-ND license (http://creativecommons.org/licenses/by-nc-nd/4.0/)
Peer review under responsibility of Chongqing University

Keywords: Nanomechanics; Dislocation; Molecular dynamics; Nanocrystalline; Magnesium.

# 1. Introduction

The pure metal magnesium (Mg) is one of the lightest metals on earth with abundant distribution in the earth's crust, making Mg an auspicious base material for light-weighting of structures [1–3]. The optimum use of low-density materials and composites, along with the conventional usage of high-density high strength steel, has great significance in the transport industry [4,5]. However, the strength and stiffness of Mg remain a significant hindrance to its broader applications. Several attempts have been made to create a viable composite with heavier and stiffer materials such as light iron [6]. However, due to the lack of miscibility and inter-atomic compound between Fe-Mg, manipulating nano/micro-structure using phase transformation to get the desired property has not been possible. Through precipitation hardening process, some

E-mail address: wenwu.xu@sdsu.edu (W. Xu).

Mg-based alloys with improved strength have been developed; however, they still do not compare well with its alternative Aluminum-based alloys [7,8]. Moreover, due to the hexagonal closed packed (HCP) structure, Mg possesses poor formability as compared to aluminum (Al), which severely restricts its applications [9].

Nano-structuring can be an effective way to improve the bulk strength with well-balanced ductility of Mg metal alloys [10,11]. Nanocrystalline metals and alloys demonstrate different characteristic mechanical properties to that of their coarse-grained counterparts [12–14]. Due to the tremendous increase in computational power in recent decades, analysis of these 3D nanocrystalline materials has become a viable option to find the optimized structure for the desired properties [15]. In comparison to the coarse-grained polycrystalline materials, nanocrystalline materials show increased strengths, hardness, and toughness, but reduced elastic modulus [16]. The reason for these improved properties is attributed to the greater grain boundary fraction in nanocrystalline materials of

<sup>\*</sup> Corresponding author.

the same average composition compared to the coarse-grained polycrystalline materials. Grain boundary fraction varies with the mean grain size, and by definition [17], nanocrystalline materials have less than 100nm mean grain size. This grain size-dependent deformation mechanisms and corresponding mechanical properties in face-center cubic (FCC) nanocrystalline metals are well researched and understood [18–20]. However, due to the directional anisotropy and having fewer slip systems, the deformation mechanism in hexagonal closepacked (HCP) metals are different from that of the FCC metals [21]. At the atomic scale, the deformation process of HCP is explained in terms of normal and zonal twinning mechanisms [22], but the grain size sensitivity of the strength and deformation mechanisms of nanocrystalline Mg has rarely been studied in the nanocrystalline range (1 - 50 nm) [23]. An earlier study by Song et al. [24] covered this range with idealized 2D MD simulation, however, with increased computational capabilities and state of the art visualization techniques of MD simulation generated data, now it is possible to simulate and analyze a much larger 3D atomic system.

MD simulation has become a preferred method to study the nanocrystalline materials at the atomic scale. This is primarily due to the limitation of synthesizing undesirable and undetectable defect-free nanocrystalline materials for experimental study. At the atomic scale, negating the effect of various unavoidable defects from the experimental results and establishing a reliable structure-property relationship is difficult. MD simulations thus provide an incisive analysis tool to characterize the structure, establish the structure-property relationship, and explore the relevant mechanisms that control that relationship.

## 2. Simulation method

A series of 3D nanocrystalline Mg samples of varying grain sizes are prepared by the Voronoi tessellation method [25]. From the largest mean grain size of 45 nm to the smallest of 6.4 nm, nine samples are generated, each containing about 43 million atoms. Each model sample has a cubic shape with a dimension of  $100 \,\mathrm{nm} \times 100 \,\mathrm{nm} \times 100 \,\mathrm{nm}$ . The number of grains in the nanocrystalline samples is sufficiently large to ensure the randomness of grain orientation. For example, there are 13 grains in the sample with a mean grain size of 45 nm and 4000 grains in the sample with a mean grain size of 6.4 nm. Large-scale Atomic/Molecular Massively Parallel Simulation (LAMMPS) is used as the MD simulation tool [26]. The Embedded Atomic Method (EAM) potential function used for the simulation is developed by Wilson and Mendeleev and is widely accepted for MD simulations of mechanical properties of Mg metal and alloys [27].

Periodic Boundary Conditions (PBC) are employed at each of the boundary surfaces of the samples to simulate its bulk property. Each Mg nanocrystalline sample is relaxed at the room temperature (300 K) and 1 bar pressure with Nose/Hoover type of sampling by the isothermal-isobaric (NPT) ensemble to attain their equilibrium configurations [28,29]. The required relaxation time increases with the de-

crease of the mean grain size of the sample. MD relaxation time of 50 ps is sufficient to equilibrate the nanocrystalline sample with a mean grain size of 45 nm. However, 120 ps is needed to relax the nanocrystalline sample with a mean grain size of 6.4 nm due to a large volume fraction of grain boundary atoms. Fig. 1(a) and (b) show the equilibrium configuration of the nanocrystalline sample of mean grain size 6.4 nm and 45 nm, respectively. It is also noticeable from Fig. 1 that with the larger grains, the shape of the grain is polyhedral, while for smaller grains, the shape of the grain becomes spherical-like, which is consistent with experimental transmission electron microscopy (TEM) observation [12].

# 3. Results and discussions

# 3.1. Overview of deformation

The MD simulation of deformations of the nine nanocrystalline Mg samples of varying grain size is carried out along the x-direction (see Fig. 1). For simulating the uniaxial tensile load along the x-direction, a response of  $10^{10}$  s<sup>-1</sup> engineering strain rate is applied with PBC in all directions. The sample was deformed until 50% of the elongation was reached, i.e.,  $\varepsilon = 0.5$ . For achieving uniform strain, the deformation timestep was split into several small time-steps. For this simulation, each deformation time-step was of 1 femtosecond (fs) in which the nanocrystalline Mg sample is scaled to 1.01 of its previous dimension and then is allowed to relax. This re-scaling and the relaxing procedure are then repeated until the desired uniaxial strain is achieved. While the deformation is carried out along x-direction, the boundary surfaces normal to y and z-direction are kept at 1 bar constant pressure [30]. The same procedure of deformation was carried out for all nine nanocrystalline Mg samples, and modeled values of stress and atomic time history were obtained as results. The software Open Visualization Tool (OVITO) is used to visualize the atomic configurations and perform dislocation quantifications [31].

# 3.2. Tensile nanomechanics and deformation mechanism

In OVITO, the Common Neighbor Analysis (CNA) method is applied to the atoms to mark their native crystal structure [32]. CNA is a crystal structure analysis algorithm that employs complex high dimensional signatures to identify the native crystal environment of the arrangements of atoms that are usually better at distinguishing between several structures [33]. Hence this method is useful for the characterization of nanocrystalline Mg where the grain interior atoms have an HCP crystal structure, grain boundary and dislocation atoms have a disordered structure, and stacking faults are identified by their FCC crystal structures [24].

The stress-strain curves of the nine nanocrystalline Mg samples reveal distinct tensile behavior from smaller to larger grain sizes (details will be provided in Section 3.4). The difference in these tensile profiles is most noticeable in the sample of 6.4 nm and 45 nm, which suggests that the deformation

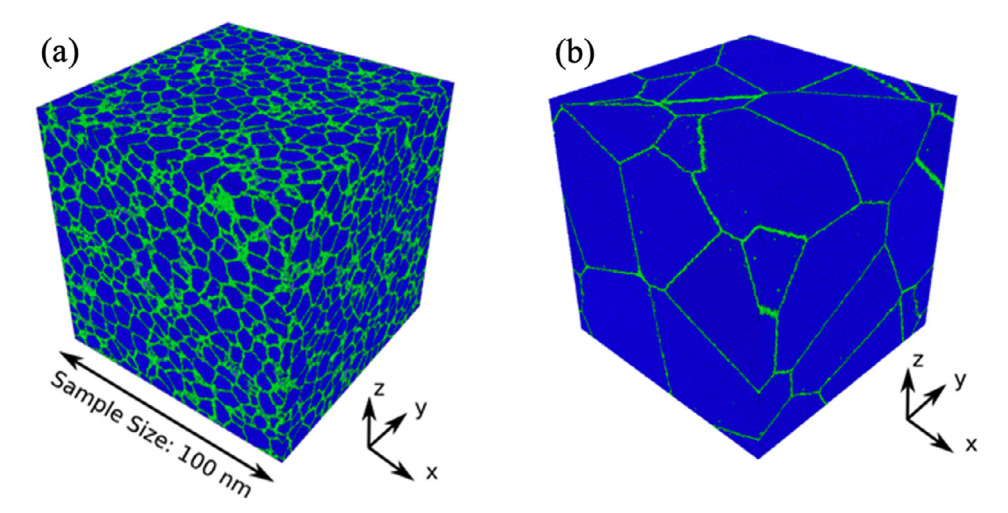


Fig. 1. Bulk Mg nanocrystalline sample with a mean grain size of 6.4 nm (a) and 45 nm (b). The blue and green regions indicate the grain interiors and grain boundaries, respectively.

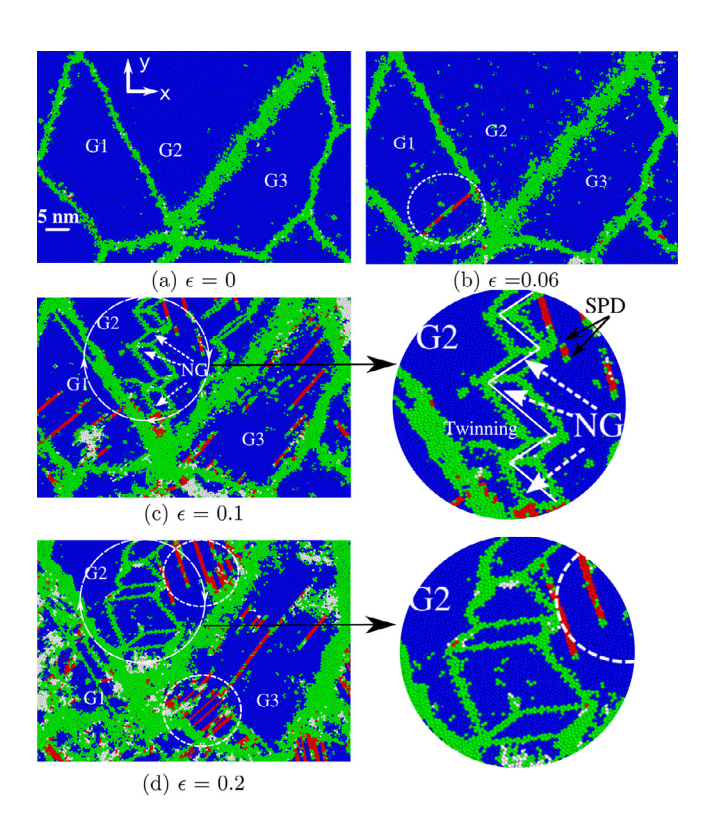


Fig. 2. Atomic microstructures of the sample with a mean grain size of 45 nm at varied strains: (a)  $\varepsilon$ =0.0, (b)  $\varepsilon$ =0.06, (c)  $\varepsilon$ =0.1, and (d)  $\varepsilon$ =0.2. Blue, green, red, and white atoms represent the HCP structure, grain boundaries or dislocations, FCC structure (stacking faults), and the intermediate BCC structure in transition, respectively. G1, G2 and G3 denote the three grains that are observed. The local structures of (c) and (d) shown on the right highlight the twinning activity and formation of nanograin (NG) twins.

in these two samples is primarily governed by two distinct deformation mechanisms. Fig. 2 shows the gradual change in the atomic microstructure of the nanocrystalline Mg sample with a mean grain size of 45 nm. The views of the plane shown in Fig. 2 are parallel to the deformation direction. The

transition from elastic to plastic deformation occurs between  $0.02 \le \varepsilon \le 0.06$  (as will be shown in Section 3.4). Fig. 2(a) shows the undeformed microstructure in a local region of the sample with a mean grain size of 45 nm. Fig. 2(b) displays the nucleation of a Shockley partial dislocation (SPD) carrying an FCC structure stacking fault at the beginning of plastic deformation as indicated by the white-dashed-circle in grain G1. The approach to determine the dislocation types will be explained in Section 3.3. The observed SPDs in the nanocrystalline Mg samples have been identified, gliding on the densely packed basal  $\{0001\}$  planes [34]. The dislocations nucleate from the grain interior and disappear/sink at the adjacent grain boundaries.

Fig. 2(c) shows the formation of new nanograin (NG) twins inside an existing grain G2, exhibiting another type of intragranular deformation mechanism. The formation of NG twins is the result of the accommodation of the c-axis strain for HCP crystals. This is because certain twin-partials possess a lower energy barrier than that of the  $\langle c+a \rangle$  pyramidal dislocation that has the lowest energy barrier among all the nonbasal dislocations in HCP structure. These twin partials predominantly possess the Burgers vector of <1011> crystal orientation [35]. Therefore, twinning activity is observed as one of the main deformation mechanisms for accommodating the c-axis strain in Mg, as shown in Fig. 2(c) and 2(d). As an example highlighted in the local enlargement of Fig. 2(c), the twinning activities in grain G2 are accompanied by the SPD formation nearby. We also observed the pile-ups of stacking faults formed by the split-up of SPDs, as indicated within the white-dashed-circles in Fig. 2(d). The stacking faults pin down the grain boundaries restricting them from sliding; as a consequence, dislocation nucleation becomes the favored mode of deformation.

However, as the nucleation and mobility of basal dislocations reduce with decreasing the crystallite size, the need for twinning to be a mechanism to accommodate the c-axis strain also reduces. Hence, the twin formation and growth as well

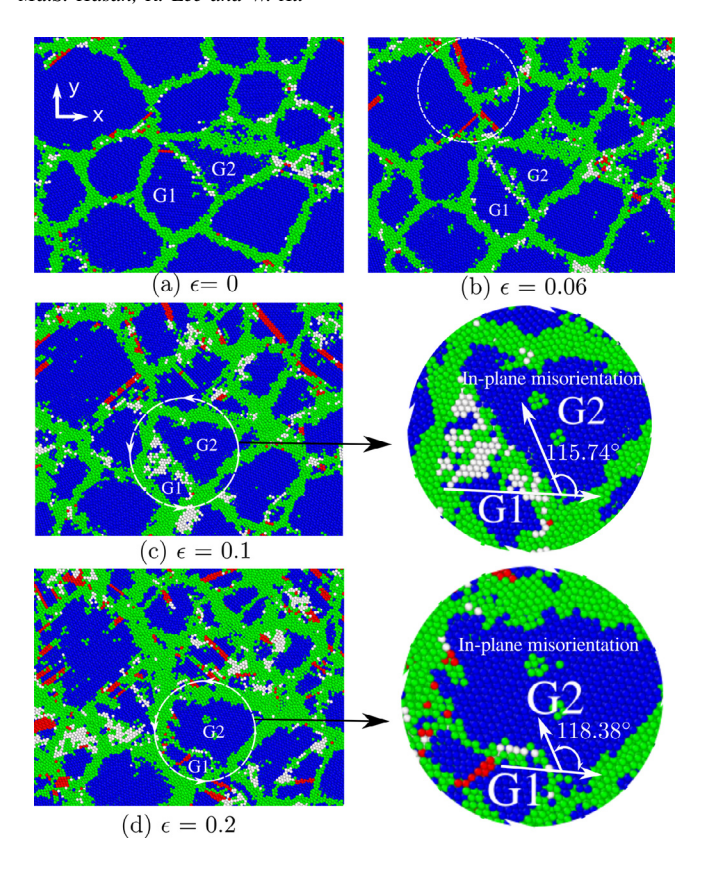


Fig. 3. Atomic microstructure of sample with a mean grain size of 6 nm at varied strains: (a)  $\varepsilon$ =0.0, (b)  $\varepsilon$ =0.06, (c)  $\varepsilon$ =0.1, and (d)  $\varepsilon$ =0.2. Blue atoms – HCP structure; green atoms – grain boundaries and dislocations; red atoms – stacking faults with FCC structure; white atoms – intermediate BCC structure. G1 and G2 represent two adjacent grains. White dashed circle in (b) shows the nucleation of dislocation from the grain boundary near the yield point, the arrow-ed circles in (c) and (d) highlight the sliding of G2 over G1.

as slipping-twinning interaction become less significant with the reduction of grain size. In the present work, only samples with average grain sizes of 45 nm and 40 nm exhibit evidence of NG twins and subsequent growth (see Fig. 2c and 2d), no evidence of twinning is observed in the nanocrystalline Mg with smaller grain sizes.

Obviously, the formation and growth of NG twins facilitate the release of strain energy, thus reducing the resistance to deformation. Thus, a rapid decrease in stress is observed near  $\varepsilon = 0.1$  in the stress-strain curve of the sample with a grain size of 45 nm (see Fig. 5i). Fig. 2(d) shows a snapshot of the atomic microstructure for a near saturation of dislocations and the subsequent stacking fault formation inside the grain interiors. Further plastic deformation does not increase the dislocation density in the sample; the corresponding quantification analysis of dislocations will be discussed in Section 3.3 (see Fig. 4a). The sustained dislocation mobility is accompanied by the growth in the NG twins to accommodate some deformation stress (see the local enlargement of Fig. 2d).

Fig. 3 shows the deformation of nanocrystalline Mg sample with a mean grain size of 6.4 nm, which has a large vol-

ume fraction of grain boundary atoms. Mostly intergranular deformation mechanism is observed where the grain boundary atom plays a dominant role in the deformation process. Fig. 3(a) shows an undeformed ( $\varepsilon = 0$ ) microstructure where the distances between the triple points are significantly smaller than that in the sample with the grain size of 45 nm. Fig. 3(b) shows the microstructure at  $\varepsilon = 0.06$ , which is at the beginning of the plastic deformation. Shockley partial dislocations are observed attached to the stacking fault, which is similar to that observed for the sample with the grain size of 45 nm. However, small nanograin size limits the mean free path for the dislocation mobility. Hence rapid dislocation generation and propagation become more difficult within the sample with a grain size of 6.4 nm as compared with that in the sample with the grain size of 45 nm. This phenomenon is further supported by Fig. 4a (details will be provided in Section 3.3), where dislocation density in the 6.4nm grainsized sample increases only slightly between  $0.06 \le \varepsilon \le 0.2$ until the dislocation density reaches a saturation.

Fig. 3(c) shows the microstructure at  $\varepsilon$  = 0.1, no significant increase in the SPD formation is observed. As there is no considerable amount of formation and mobility of basal dislocation, the consequent intra-granular twinning activity is absent. Instead, the grain boundary rotation and sliding are appeared to dominate the deformation process. For example, from the local enlargements of Fig. 3(c) and 3(d), we observed a 2.64° =(118.38°-115.74°) difference in the in-plane misorientation angle between grain G2 and grain G1 as the strain increases from 0.1 to 0.2. The interface atoms between G1 and G2 are subjected to shear, indicated by their temporary BCC crystal structure (see the local enlargement of Fig. 3c) caused by the change in the in-plane grain misorientation and the relative rotation between the G1 and G2.

It is worth mentioning that the nanosize effect on tensile deformation in nanocrystalline Mg is largely different from that in the nanocrystalline Al, attributed to their different crystal structures. The HCP Mg has a stacking fault energy of 125 mJ/m<sup>2</sup> [36], which is lower than that of the FCC Al (160–200 mJ/m<sup>2</sup>) [37]. Because of the lower stacking fault energy along with the inadequate slip systems in HCP structure, the deformation of Mg creates more partial dislocations and twins instead of full dislocations [38], unlike Al. New stacking faults are easily created in Mg due to differences in the dislocation velocity of the leading and trailing partial dislocation [38]. While the partial dislocation sinks into the grain boundary, these stacking faults piles up against the grain boundary providing additional resistance to inter-granular mechanisms like grain-sliding and grain rotation. As a result, at the nanoscale, the grain boundary rotation and sliding become the dominant mechanisms in nanocrystalline Mg at a very small grain size level (< 10 nm), in contrast to that for nanocrystalline Al (< 25 nm) [18].

# 3.3. Dislocation quantifications

Dislocation Extraction Algorithm (DXA) in OVITO is used for the identification of dislocation defects as line

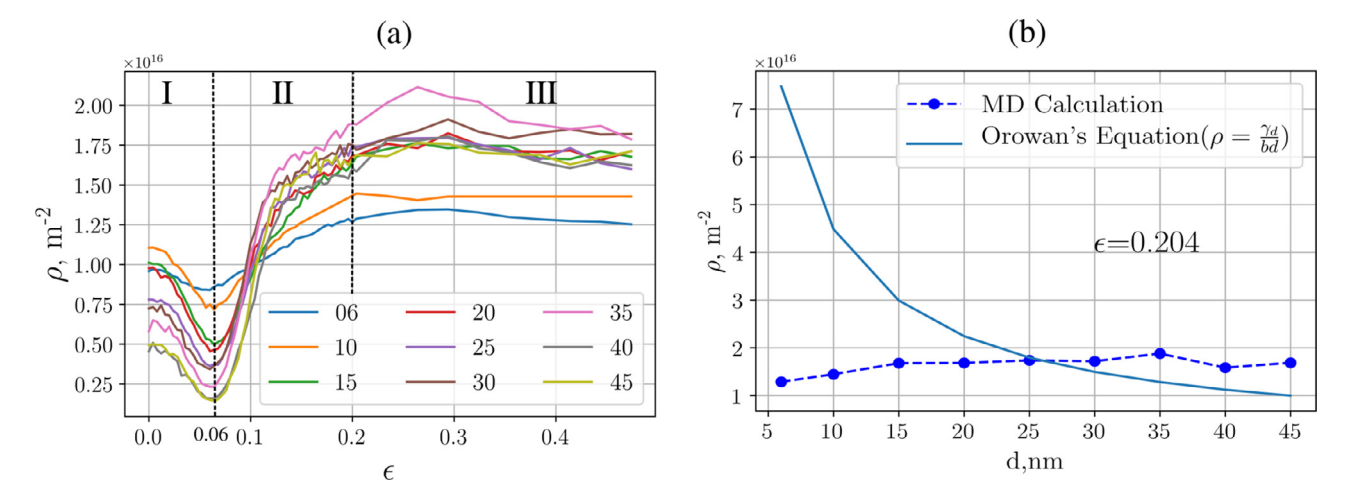


Fig. 4. (a) Dislocation density as a function of strain  $(\varepsilon)$  for the nine nanocrystalline Mg samples with varying grain sizes, (b) the breakdown of Orowan's dislocation density model at an ultrafine nanograin size.

representation [39,40]. The line segment representation of the dislocation is obtained for all the nanocrystalline Mg samples. Dislocation density is obtained by dividing the total line length by the instantaneous cell volume for each strain state. DXA also identifies the Burgers vector of the dislocation to classify the type of dislocations. It is found that, during the tensile deformation of nanocrystalline Mg, the Shockley partial dislocation is the most common type and the perfect dislocation as the second most dominant type. This observation is consistent with previously reported single-crystal studies of Mg, where dislocation-based deformation occurs by predominantly the Shockley partials and perfect dislocations gliding across the closed packed basal {0001} planes [22,34]. Also, it is reported in the literature that only the basal plane is activated at room temperature during the deformation of Mg, while the prismatic and pyramidal planes can be thermally activated above 393 K [34].

Fig. 4(a) presents the dislocation density as a function of strain for each sample, which can be identified into three distinct regions. It is noticed that there are varying amounts of residual dislocation (concentrated at grain boundary regions) in all the nanocrystalline samples at zero strain conditions. In region I, dislocation density reduces with the increase of strain within the elasticity region ( $\varepsilon \approx 0$  - 0.06). This phenomenon is expected as within the elastic region, dislocation annihilation takes place without the creation of any new dislocations. Dislocation density reaches its minimum at the yield point ( $\varepsilon \simeq 0.06$ ). Beyond the yield point (region II), dislocation density starts increasing abruptly. This rapid increase is associated with the creation and multiplication of new dislocations when the plastic deformation takes place. As the strain further increases (region III), dislocation density reaches its maximum and then stabilizes to a constant value. This is also expected, as there is a limiting value of dislocation density in a material at equilibrium for a particular temperature [41].

Moreover, as the grain size in the sample reduces from 45 nm to 6.4 nm, the variation in dislocation density during the plastic deformation reduces significantly. This phe-

nomenon can be explained by the transition of deformation mechanism from dislocation dominated to grain boundary dominated. For the nanocrystalline sample with a mean grain size of 45 nm, the deformation is dislocation dependent; thus, a large difference in the dislocation densities between the yield point ( $\sim 2 \times 10^{15}$  m<sup>-2</sup>) and stabilization region ( $\sim 1.7 \times 10^{16}$  m<sup>-2</sup>) is observed. In contrast, for the 6.4 nm grain-sized sample where the grain boundary dependent deformation mechanism is dominated, the dislocation density shows a relatively small change in the dislocation density between the yield point ( $\sim 0.8 \times 10^{16}$  m<sup>-2</sup>) and the stabilization region ( $1.3 \times 10^{16}$  m<sup>-2</sup>).

Contribution to strain from the dislocation can be considered as an independent contribution  $\gamma_d$  to the total strain  $\gamma_t$  from the other deformation mechanisms [42] and a dislocation density profile can be obtained analytically from the Orowan's equation as follows,

$$\gamma_d = \rho l b \tag{1}$$

where  $\rho$  is the dislocation density, l is the dislocation free path which is assumed to be equal to the grain size d. Burgers vector b is equal to a (the basal lattice distance) for the perfect dislocations and  $\frac{1}{3}a$  for the Shockley partial dislocations. Using Eq. (1), we can compute the dislocation density as a function of grain size in nanocrystalline Mg with considering only the dislocation dominated deformation mechanism.

Fig. 4(b) shows the comparison of the stabilized/equilibrium dislocation density obtained from present MD simulations with the Orowan's dislocation density equation at  $\varepsilon = 0.204$  (the starting strain at which equilibrium dislocation density is reached for all samples, see Fig 4a). Orowan's equation compares well with the MD result at and above 25 nm grain-sized samples. For smaller grain-sized samples, however, the Orowan's equation severely overestimates dislocation density compared to MD result. This result further supports the existence and predominance of an alternative deformation mechanism i.e., the grain boundary sliding-rotation in the ultrafine nanocrystalline Mg.

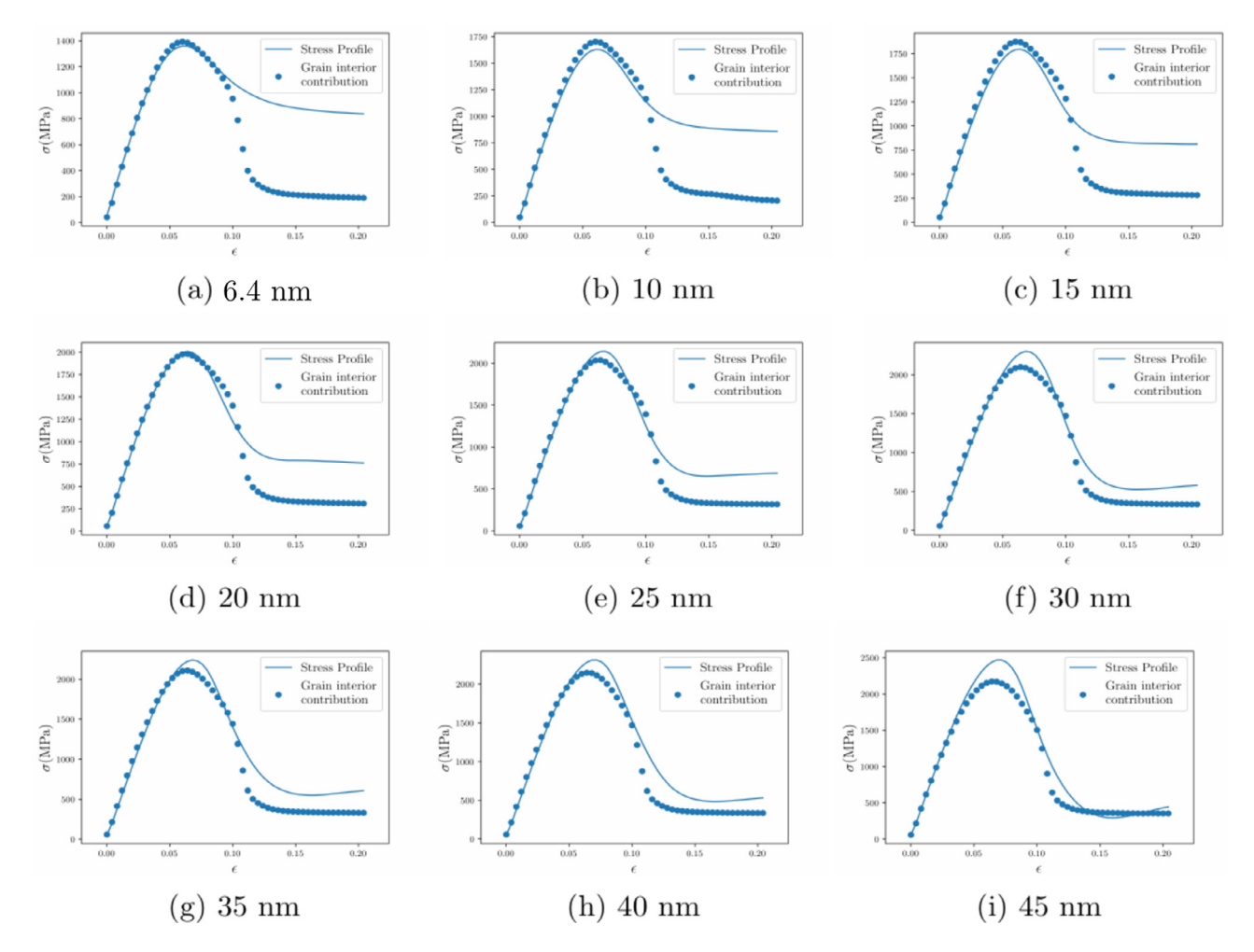


Fig. 5. Gradual transition from grain boundary dominated stress profile to dislocation dominated stress profile in nanocrystalline Mg system.

# 3.4. Size dependence of mechanical properties

Fig. 5 describes the gradual transition from grain boundary dominated stress profile to a dislocation dominated stress profile in the nanocrystalline Mg. Uniaxial tensile deformations are carried out in a single crystal Mg sample by applying loading at <0001> and <1010> directions using MD simulations. From which, two distinct stress-strain profiles are obtained for the single crystal with different orientations. Since the single crystal does not have grain boundaries at its initial configuration, the deformation mechanism can be assumed to be purely dislocation dominated. Then, a weighted average of the stress-strain curve is taken considering contributions from the (0001) and  $<10\overline{10}>$  crystal orientations. This is to generate an approximated stress-strain profile solely due to the dislocations. The pure dislocation dominant stress profile is further scaled to the fraction of grain interior atoms in the undeformed models to obtain the approximated stress contribution from the grain interior in the stress-strain profile at the respective grain size, as the results denoted by the dotted curves.

We then compare these stress profiles by grain interior contributions with the MD stress profiles (solid curves). As seen in Fig. 5, the elastic region of the MD stress profile

(solid curve) of each sample overlaps with the pure dislocation dominated stress profile (dotted curve) since no plastic deformation takes place. This overlapping at the elastic region validates the above-mentioned approximation model of stress profile. Interestingly, in the plastic deformation region ( $\varepsilon$  >  $\sim 0.05 - 0.06$ ), the stress profiles of the smallest grain-sized sample (Fig. 5(a), 6.4 nm) is distinctly different to that of the largest grain-sized sample (Fig. 5(i), 45 nm) in the nanocrystalline Mg. This difference can be attributed to the different plastic deformation mechanisms, as described in the previous sections. For example, the most significant difference in the plastic region between the actual MD stress profile (solid curve) and the approximated stress profile (dotted curve) is observed in the nanocrystalline Mg with a mean grain size of 6.4 nm. This implied that the plastic deformation mechanism in the 6.4 nm grain-sized sample largely deviates from the dislocation dominated mechanism, which is consistent with our previous observations (see Fig. 3). As the grain size increases, the stress profile increasingly follows the trends of dislocation dominated stress profiles, indicating a gradual change is the deformation mechanism.

Fig. 6 shows the normal and inverse Hall-Petch relationship in terms of the flow stress for the grain size range, which is consistent with the earlier findings of the nanocrystalline

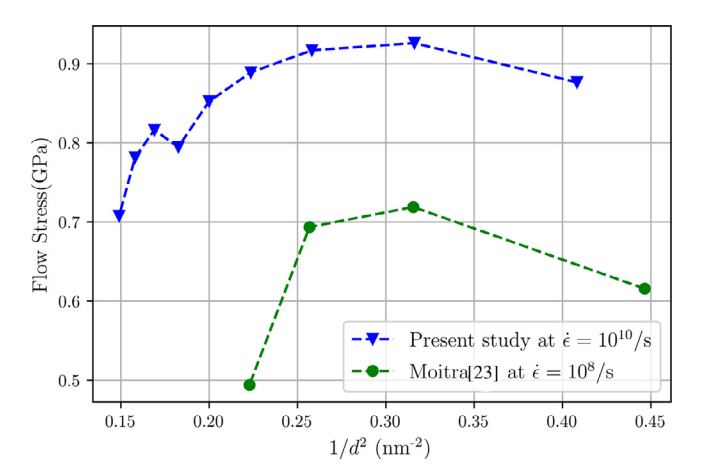


Fig. 6. Hall-Petch relationship of the flow stress in the nanocrystalline Mg system.

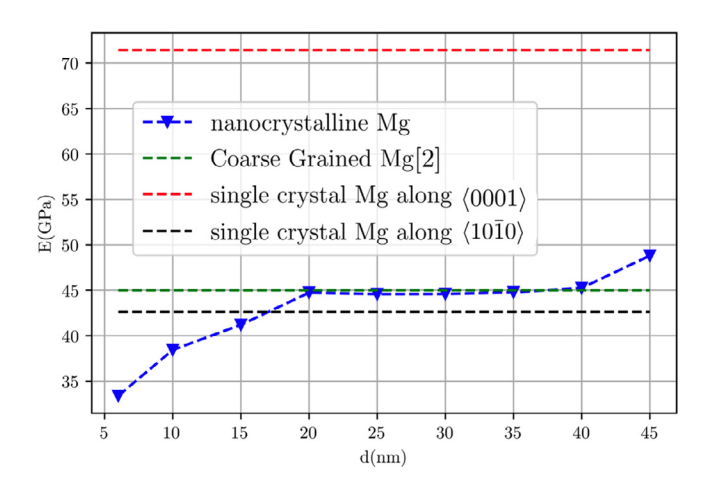


Fig. 7. Elastic modulus of the nanocrystalline Mg as a function of grain size as compared to that in the single crystal with loading at  $\langle 0001 \rangle$  direction (normal to the basal plane) or at  $\langle 10\bar{1}0 \rangle$  direction (parallel to the basal plane) as well as the coarse-grained bulk counterparts.

Mg sample in the range of 5 nm to 30 nm [23]. The higher absolute flow-stress values in the present work are due to the 100 times larger strain rate used in our MD simulation compared to the previous study. Nanocrystalline Mg with a mean grain size of 10 nm can be identified as an optimum grain size for maximum strength, which also marks the transition between the normal and inverse Hall-Petch curve. The grain size dependence of elastic or Young's modulus is depicted in Fig. 7. When the mean grain size in nanocrystalline Mg is above about 20 nm, Young's modulus remains comparable to that of the coarse-grained Mg. We also computed the anisotropy of elastic modulus of single-crystal Mg at directions parallel or normal to the basal plane. As expected, the elastic modulus of the coarse-grained Mg lies between the two values of elastic moduli of single-crystal Mg at the (0001) and <1010> orientations. Below 20 nm, Young's modulus is highly sensitive to the grain size and decreases rapidly with the further reduction of grain size. This observation is consistent with the continuum theory based modeling result that the effective elastic modulus decreases and effective Poisson ratio increases below a certain threshold in nanocrystalline bulks [43].

# 4. Conclusions

In this work, the grain size effect on the deformation of nanocrystalline Mg was systematically investigated by MD simulations. The main conclusions are summarized as follows:

- (1) Two distinct nanomechanics are dominating the deformation in nanocrystalline Mg: the dislocation-based mechanism at larger grain sizes ( $> \sim 25 \, \text{nm}$ ) and the grain boundary-based mechanism (grain boundary sliding/grain rotation) at smaller grain sizes ( $< \sim 10 \, \text{nm}$ ).
- (2) There is a gradual transition in the deformation mechanism from dislocation-based to a non-dislocation-based with the reduction of grain size in the nanocrystalline Mg.
- (3) The transition of normal and inverse Hall-Petch relation for flow stress was determined to be ∼10 nm for the nanocrystalline Mg. The elastic modulus of nanocrystalline Mg decreases rapidly when the grain size is reduced to below 20 nm.

In summary, the grain-boundary based mechanism reported in the present work may provide a potential remedy for the poor formability of Mg-based metal alloys. The overall work may provide essential fundamental knowledge for the future development of high performance Mg-based nanocrystalline alloys.

# Acknowledgments

This work was performed under the auspices of startup funds from the San Diego State University (SDSU) and the support of the US National Science of Foundation, Division of Materials Research, under Award No. 1900876. The authors wish to thank the High-Performance Computing Cluster (HPCC) at SDSU for providing computing support for this project.

# References

- [1] T.M. Pollock, Science 328 (2010) 986-987.
- [2] B.L. Mordike, T. Ebert, Mater. Sci. Eng. A. 302 (2001) 37-45.
- [3] T. Xu, Y. Yang, X. Peng, J. Song, F. Pan, J. Magnes. Alloy. 7 (2019) 536–544.
- [4] K. Lu, Science 328 (2010) 319-320.
- [5] M. Zha, H.M. Zhang, Z.Y. Yu, X.H. Zhang, X.T. Meng, H.Y. Wang, Q.C. Jiang, J. Mater. Sci. Technol. 34 (2018) 257–264.
- [6] S. Gorsse, M. Prakasam, S. Couillaud, O. Bouaziz, J.L. Bobet, P. Bellanger, Mater. Sci. Eng. A. 651 (2016) 987–990.
- [7] J.F. Nie, Metall. Mater. Trans. A Phys. Metall. Mater. Sci. 43 (2012) 3891–3939.
- [8] F.X. Wang, B. Li, J. Magnes. Alloy. 6 (2018) 375-383.
- [9] K.K. Alaneme, E.A. Okotete, J. Magnes. Alloy. 5 (2017) 460-475.
- [10] Y. Dong, I.W. Chen, J. Am. Ceram. Soc. 98 (2015) 3624-3627.
- [11] A. Mahata, K. Sikdar, J. Magnes. Alloy. 4 (2016) 36–43.
- [12] H. Gleiter, Acta Mater. 48 (2000) 1-29.
- [13] W. Xu, X. Song, N. Lu, C. Huang, Acta Mater. 58 (2010) 396-407.

- [14] X. Song, Y. Gao, X. Liu, C. Wei, H. Wang, W. Xu, Acta Mater. 61 (2013) 2154–2162.
- [15] G.P. Zheng, Y.M. Wang, M. Li, Acta Mater. 53 (2005) 3893–3901.
- [16] C. Suryanarayana, Bull. Mater. Sci. 17 (1994) 307-346.
- [17] R. Birringer, Mater. Sci. Eng. A 117 (1989) 33-43.
- [18] W. Xu, L.P. Dávila, Mater. Sci. Eng. A 692 (2017) 90-94.
- [19] W. Xu, L.P. Dávila, Mater. Sci. Eng. A 710 (2018) 413-418.
- [20] T. Shimokawa, A. Nakatani, H. Kitagawa, Phys. Rev. B Condens. Matter Mater. Phys 71 (2005) 224110.
- [21] J. Wang, I.J. Beyerlein, N. Mara, A. Misra, C.N. Tome, in: Proceedings of the Conference Program for the 3rd International Conference on Heterogeneous Materials Mechanics., 2011, pp. 88–91.
- [22] J. Wang, J.P. Hirth, C.N. Tomé, Acta Mater. 57 (2009) 5521-5530.
- [23] A. Moitra, Comput. Mater. Sci. 79 (2013) 247-251.
- [24] H.Y. Song, Y.L. Li, J. Appl. Phys. 111 (2012) 044322.
- [25] P. Hirel, Comput. Phys. Commun. 197 (2015) 212-219.
- [26] S. Plimpton, J. Comput. Phys. 117 (1995) 1-19.
- [27] S.R. Wilson, M.I. Mendelev, J. Chem. Phys. 144 (2016) 144707.
- [28] W.G. Hoover, Phys. Rev. A. 31 (1985) 1695-1697.
- [29] S. Nosé, Mol. Phys. 52 (1984) 255-268.
- [30] M. Parrinello, A. Rahman, J. Appl. Phys. 52 (1981) 7182-7190.
- [31] A. Stukowski, Model. Simul. Mater. Sci. Eng. 18 (2010) 015012.

- [32] D. Li, F.C. Wang, Z.Y. Yang, Y.P. Zhao, Sci. China Physics, Mech. Astron. 57 (2014) 2177–2187.
- [33] A. Stukowski, Model. Simul. Mater. Sci. Eng. 20 (2012) 45021.
- [34] K. Fukuda, Y. Koyanagi, M. Tsushida, H. Kitahara, T. Mayama, S. Ando, Mater. Trans. 58 (2017) 587–591.
- [35] C.D. Barrett, H. El Kadiri, M.A. Tschopp, J. Mech. Phys. Solids. 60 (2012) 2084–2099.
- [36] N.V. Ravi Kumar, J.J. Blandin, C. Desrayaud, F. Montheillet, M. Suéry, Mater. Sci. Eng. A 359 (2003) 150–157.
- [37] B. Hammer, K.W. Jacobsen, V. Milman, M.C. Payne, J. Phys. Condens. Matter. 4 (1992) 10453–10460.
- [38] R.E. Smallman, D. Green, Acta Metall. 12 (1964) 145-154.
- [39] A. Stukowski, K. Albe, Model. Simul. Mater. Sci. Eng. 18 (2010) 085001.
- [40] A. Stukowski, V.V. Bulatov, A. Arsenlis, Model. Simul. Mater. Sci. Eng. 20 (2012) 085007.
- [41] K. Nakashima, M. Suzuki, Y. Futamura, T. Tsuchiyama, S. Takaki, Mater. Sci. Forum. 503–504 (2006) 627–632.
- [42] Y. Tang, E.M. Bringa, M.A. Meyers, Mater. Sci. Eng. A 580 (2013) 414–426.
- [43] Int. J. Solids Struct. 49 (2012) 3942-3952.